Electrical Transport Properties of Highly Doped N-Type GaN Materials

L Konczewicz, E Litwin-Staszewska, M Zajac, H Turski, M Bockowski, D Schiavon, M Chlipala, M Iwinska, P Nita, S Juillaguet, et al.

Electrical Transport Properties of Highly Doped N-Type GaN Materials

L. Konczewicz[1,2], E.Litwin-Staszewska[1], M.Zajac[1], H.Turski[1], M.Bockowski[1], D.Schiavon[1], M. Chlipała[1], M. Iwinska[1], P.Nita[1], S. Juillaguet[2] and S. Contreras[2]

[1] Institute of High Pressure Physics, Polish Academy of Sciences, Warsaw, PL 01 142, Poland
[2] Laboratoire Charles Coulomb (L2C), University of Montpellier, CNRS, F 34 095, Montpellier, France

E-mail: leszek.konczewicz@unipress.waw.pl

Received xxxxxx
Accepted for publication xxxxxx
Published xxxxxx

Abstract

This paper presents a comparative study of electron transport phenomena in n-type gallium nitride strongly doped, above the Mott transition, with silicon and germanium. The samples under study were grown by molecular beam epitaxy, metal-organic vapor phase epitaxy and halide vapor phase epitaxy. The temperature dependence of resistivity and Hall Effect was investigated at temperatures ranging from 10 K up to 650 K. The measurements at sub-room temperatures allow the study of scattering mechanisms related to extrinsic material properties. The observed temperature dependences of the electrical transport properties were analyzed in the frame of the model taking into account a typical scattering mechanism and degree of degeneracy of free carrier electron gas. The limitations of the applied models will be presented.

Keywords: n-type GaN, heavily doped, electrical transport phenomena, mobility

1. Introduction

Nowadays the applications of gallium nitride (GaN) and related compounds-based devices are very broad, from light emitting devices to high power transistors. The number of these applications have continuously increased over the last decade, making nitride materials the second semiconductor market in volume after silicon (Si) technology. High impurity doping via extrinsic sources is the key for fabrication of optical and electronic devices. For a long time Si was the most common n-type GaN dopant, as it readily incorporates on a Ga-site forming a single shallow donor and leading to a nearly complete donor ionization at room temperature. For a low silicon concentration limit, the Si binding energy tends to E_0 = 27 meV and with increasing the doping level this energy tends to zero at the critical concentration of about 1.6×10^{18} cm^{-3} [1]. The growth of Si-doped GaN is largely controlled over a wide range of carrier densities from low-10^{17} to mid-10^{19} cm^{-3}. However, some structural problems occur in heavily doped films. For this reason, over time, germanium (Ge) became the second competitor of *n*-type doping [2]. While doping GaN to low and

intermediate concentrations using Si and Ge has become routine, compensation mechanisms are activated under very high donor doping, limiting the maximum electron concentration achievable with either dopant. Basing on theoretical studies [3] this effect can be explained by the creation of multi-member Ga/Si vacancy-donor substitutional complexes under degenerate doping conditions. The differing energetics of Ge- and Si-related complexes ultimately suggests Ge as the more effective donor in degenerate conditions. To compare both types of doping elements the available bibliographic results of the electrical properties of *n*-type GaN are presented in Fig. 1, where data for three basic GaN growth technologies: molecular beam epitaxy (MBE), metal-organic vapor phase epitaxy (MOVPE) and halide vapor phase epitaxy (HVPE) are summarized. The figure shows the mobility (Fig. 1A) and conductivity (Fig. 1B) of GaN as a function of the concentration of free electrons. While the mobility is a parameter that allows to assess the electrical quality of the material under study, conductivity is a quantity directly related to the use of the material in the devices.

seems to be better than for Ge as the *n*-type dopant. For a given free carrier concentration, both mobility and conductivity for Si-doped samples are higher than those in the Ge-doped ones. For the purpose of fitting the $\sigma(n)$ data for both Si and Ge shallow donors Narita proposed [4] the following relation: $\sigma(n)=1/\rho$ with $\rho=1.247\times10^{12}\times n^{-0.7675}$. It is shown in Fig. 1B as a solid line.

The situation is particular for the highest available concentrations. Although the use of Ge allows for a much higher free carrier concentration, the obtained conductivity values are not higher than those for significantly lower Si-doping level. This general conclusion does not raise any doubts, however, it is important to consider separately the case of different techniques for material growth: MOVPE, MBE and HVPE. It will be done in Part III.

In this paper, the electrical characterization of highly doped *n*-type GaN with carrier concentration $n>1\times10^{18}$ cm^{-3} is presented. The samples under study were prepared from GaN grown using three basic techniques: MOVPE, plasma-assisted MBE (PAMBE), and HVPE. In all the cases, *n*-type material was obtained by doping with Ge. Layers doped with Si were grown by PAMBE and HVPE.

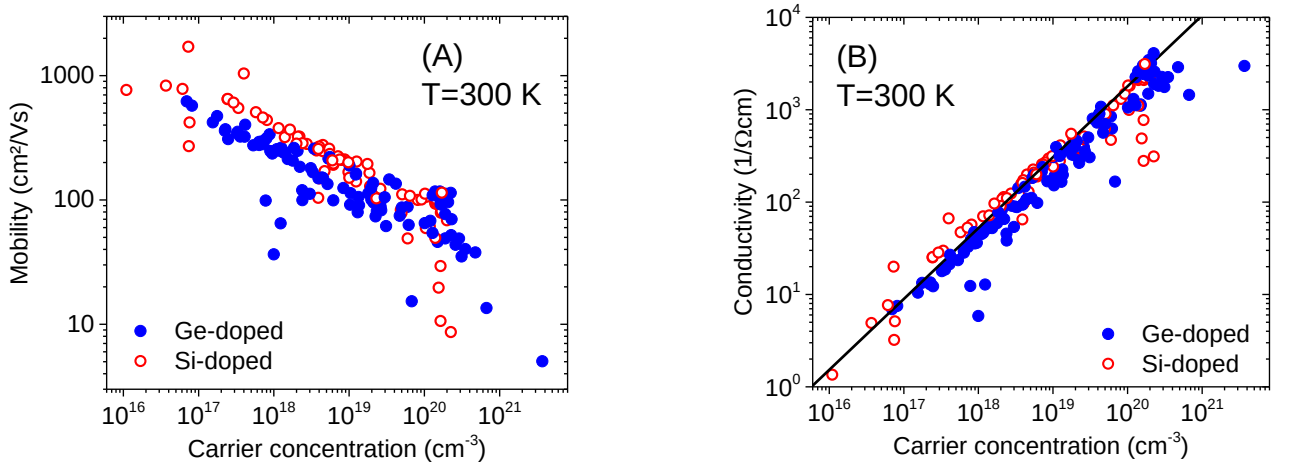

Fig. 1 Bibliographic data [5-23] on the mobility (1A) and conductivity (1B) of Si- (open, red circles) and Ge-doped (full, blue circles) *n*-type GaN. The solid line correspond to fitting $\sigma(n)$ dependency proposed by Narita for both Si and Ge shallow donors [4].

From both Fig. 1A and 1B it is clearly visible that in the whole wide range of concentration, the parameters of the obtained material doped with Si

For all the investigated samples material parameters at room temperature were determined from resistivity and Hall Effect measurements.

Additionally, for several samples, measurements were performed as a function of temperature in the range from 650 K down to 10 K.

The scattering of electrons by phonons can be considered as independent on the free carrier concentration [24]. Therefore, the phonon limited mobility $\mu_{ph}(T)$ is characteristic for each semiconductor and is independent on the doping level. The scattering mechanisms associated with lattice vibration are, by their nature, effective with increasing temperature. For GaN the mechanisms of carrier scattering by phonons become dominant at high temperatures, starting from room temperature [24]. Therefore carrying out measurements below room temperature enables the study of scattering mechanisms related to the external properties of materials. The electrical transport properties are analysed in the frame of the model taking into account typical scattering mechanisms. Limitations of the applied models will also be discussed.

2. Experimental methods

The samples under study were prepared from GaN grown using three basic techniques: MOVPE, PAMBE, and HVPE.

(i) The MOVPE materials under study were grown on c-plane (0001) sapphire substrates in an Aixtron close-coupled-showerhead reactor. The epitaxial structure consisted of a 5-μm thick undoped GaN buffer layer, and a GaN:Ge active layer with thickness in the range 0.5–1.2 μm. The details of growth process are described in paper [19].

(ii) PAMBE GaN under study was grown in a Gen20 Veeco MBE system equipped with a high (up to 3 μm/h) growth rate plasma source. The 284 nm thick GaN layers doped with Ge or Si were grown on templates initially prepared by MOVPE technique. All layers were grown under metal-rich conditions, typical for PAMBE [25]. In some cases indium (instead of gallium) was used as a surfactant [26] during the growth process and the sample numbers from these processes are marked in Tab. I with an asterisk. The MOVPE template structures were grown on c-plane (0001) sapphire and consists of 25 nm thick low temperature GaN nucleation layer, 1.5 μm of unintentionally doped and highly resistive GaN followed by 3.5 μm of undoped, high quality and highly resistive GaN.

(iii) HVPE samples under study were prepared from crystals grown in a home-built quartz HVPE reactor with a horizontal configuration. Native, ammonothermally-grown GaN substrates with misorientation ~0.3 degree to the m-direction were used as seeds. They all were of high structural quality [27]. The details of growth process are described elsewhere [28, 29]. The seeds were removed, leaving free-standing HVPE of the thickness of a few hundred micrometers for characterization.

All the investigated GaN samples were cut into 5 mm × 5 mm squares and electrical contacts were placed in van der Pauw configuration in the corners of each sample. Ohmic contacts were formed by the evaporation of Ti (200 nm) / Au (700 nm) electrodes and subsequent annealing in N_2 ambient at 1000 K. The samples were bonded with gold-wires to a ceramic support and installed inside a He-free cryostat enabling measurements at temperatures ranging from 10 K to 800 K. The temperature was stabilized with a precision better than 0.1 K.

The resistivity measurements were performed using the van der Pauw method taking the average of all current configurations. During all the electrical measurements, the current through the sample I_s was kept adequately low to ensure ohmic conditions. Concerning Hall Effect measurements, the van der Pauw approach [30] was used to determine the Hall voltage V_H. However, because of the low V_H values resulting from the high concentration of electrons in the samples, to improve the measurements precision they were made as a function of the magnetic field B varying up to ±1 Tesla. Then the Hall carrier concentration was deduced from the slope β of the Hall resistance $R = V_H/I_s$ versus B: $\beta = dR/dB$.

3. Electrical transport properties of highly doped n-type GaN

3.1 Room temperature characterization

The list of the investigated samples and their room temperature parameters are presented in Tab. I. The complete conductivity data for the investigated samples as well as the available bibliographic results are presented in Fig. 2. The conductivity vs concentration is shown separately for the samples under study obtained by the MOVPE (2A), MBE (2B) and HVPE (2C) techniques. The following conclusions can be made for each growth method:

(i) In the case of GaN grown by MOVPE from literature data it is clearly visible that doping with Si is limited to the free carrier concentrations up to 1.5×10^{20} cm^{-3}. Consequently the conductivity is not higher than 1×10^{3} 1/Ωcm. Obtaining material with a higher conductivity is possible only in the case of doping with Ge [23]. For the samples under study, the technological parameters applied for the Ge doping process made it possible to obtain particularly high conductivity values in the whole carrier concentration range. In the case of the most doped sample the highest conductivity value available in the literature for this technology (of about 2.5×10^{3} 1/Ωcm [23]) was obtain for a relatively low free carrier concentration.

(ii) In GaN grown by PAMBE technique it is possible to obtain the conductivity values up to about 2.9×10^{3} 1/Ωcm [10] for Ge-doped samples. Although the use of Ge allows for a higher doping level of the material. Unfortunately it does not translate into an increase in the conductivity value. For the samples under study, the applied technological process allowed to obtain Ge-doped material with conductivity values higher than 4×10^{3} 1/Ωcm for carrier concentration 3.7×10^{20} cm^{-3}. Increasing this value up to 7.9×10^{20} cm^{-3} results in no significant change in the conductivity value. However, the largest conductivity value of about 4.25×10^{3} 1/Ωcm measured in the investigated samples was also the highest one available in the literature.

(iii) In the case of GaN grown by HVPE technique, the obtained conductivity values are lower than for the two other techniques, but the technology is more reproducible (the results are less scattered). The use of the Si dopant undoubtedly allows to obtain samples with higher conductivity. However, the literature data for Ge doping [14] indicate that a proper selection of technological parameters should decrease the dislocation concentration and the level of compensating acceptors. This allows to obtain samples with $\sigma(n)$ values as high as in the case of the Si dopant. Although it should be noted that the samples investigated in paper [14] in addition to the basic Ge dopant also contained some Si co-doping. For the materials under study, using Ge as a dopant allowed to obtain the highest conductivity value reported in the literature for this growth method of the order of 1×10^{3} 1/Ωcm for carrier concentration of 6.1×10^{19} cm^{-3}.

3.2 Electrical transport properties as a function of temperature

For some samples, indicated in Tab.1 by “yes” in column ”Study of T-dependency”, the resistivity and Hall Effect were investigated as a function of temperature in the range from 10 K to almost 650 K. The analysis of the measured samples parameters of and their temperature dependence did not allow to distinguish a specific behavior of one technology or one dopant. Therefore, the results presented below are given without detailing the growth technology and the type of dopant. However, following the sample numbers, these details can be find from Tab. I.

3.2.1 Hall Effect as a function of temperature

The Hall Effect is the key measurement used in investigations of the basic electrical conduction process. The reason for this comes from the simple relation between the Hall Coefficient R_H and the free carrier concentration n in the material.

TABLE I: Sample characteristics: Hall concentration $n_H=1/(eR_H)$ and Hall mobility $\mu_H=1/(e\rho n_H)$ at 300 K. The letters in sample number: M=MOVPE; H=HVPE; P=PAMBE (*= Indium surfactant).

Sample	Growth Tech.	Dopant	n_H (cm^{-3})	μ (cm²/Vs)	Study of T-dependency
M1	MOVPE	Ge	2.0×10^{18}	276	yes
M2		Ge	2.8×10^{18}	230	yes
M3		Ge	4.1×10^{18}	216	yes
M4		Ge	6.9×10^{18}	196	yes
M5		Ge	7.3×10^{18}	202	yes
M6		Ge	1.1×10^{19}	224	no
M7		Ge	1.3×10^{19}	100	no
M8		Ge	1.8×10^{19}	90	no
M9		Ge	4.4×10^{19}	153	yes
M10		Ge	1.3×10^{20}	120	yes
P1	PAMBE	Ge	2.5×10^{18}	146	no
P2		Ge	2.5×10^{18}	278	no
P3*		Ge	1.7×10^{18}	186	yes
P4*		Ge	4.6×10^{18}	133	no
P5*		Ge	5.4×10^{18}	221	no
P6*		Ge	1.2×10^{20}	88	yes
P7*		Ge	3.5×10^{20}	66	no
P8*		Ge	3.7×10^{20}	69	no
P9*		Ge	4.5×10^{20}	43	no
P10*		Ge	5.3×10^{20}	47	yes
P11*		Ge	7.9×10^{20}	33	yes
P12		Si	8.3×10^{18}	166	yes
P13		Si	9.9×10^{18}	205	no
P14*		Si	2.4×10^{18}	181	no
P15*		Si	2.7×10^{19}	97	yes
H1	HVPE	Ge	4.1×10^{18}	184	yes
H2		Ge	8.8×10^{18}	192	yes
H3		Ge	1.6×10^{19}	127	yes
H4		Ge	6.1×10^{19}	107	yes
H5		Si	1.3×10^{18}	297	yes
H6		Si	3.1×10^{18}	246	yes
H7		Si	7.9×10^{18}	144	yes
H8		Si	1.1×10^{19}	153	yes

In the case of conduction dominated by a single charge-carrier type this relation is given by:

$$R_H = \frac{r_H}{ne} = \frac{1}{n_H e} \qquad (1)$$

where n_H is the Hall concentration and e is the charge of the carrier. The proportionality factor r_H called the "Hall scattering factor" is given by:

$$r_H = \frac{\langle\tau^2\rangle}{\langle\tau\rangle^2} \qquad (2)$$

where τ is the relaxation time for the scattering process and $\langle X\rangle$ is the average value of function X. As a result, the Hall factor r_H depends on the carriers scattering mechanisms and their statistics. In the classical regime, where the carrier density is low enough to render quantum effects negligible, the Maxwell–Boltzmann statistics can be used.

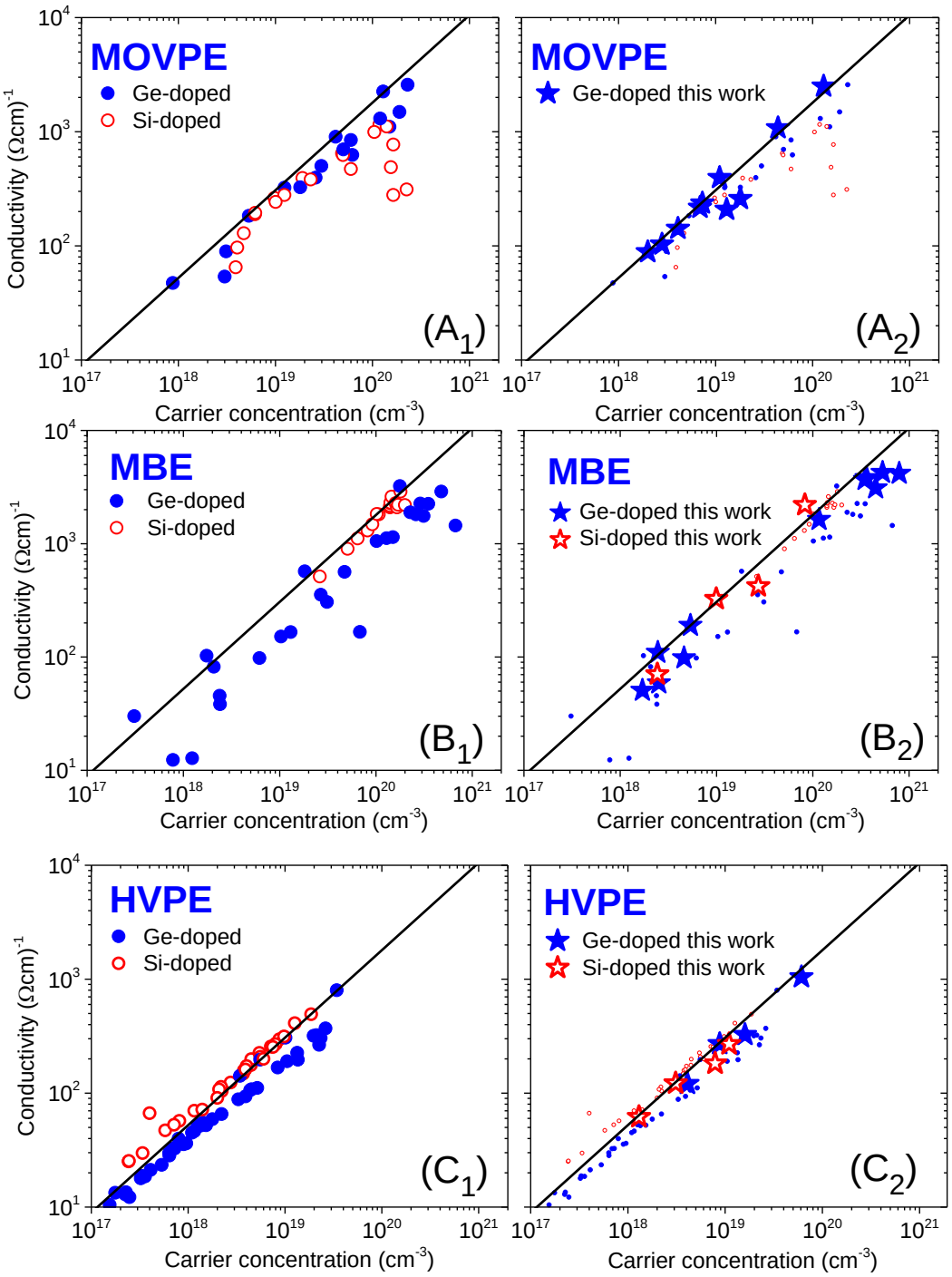

Fig. 2. GaN conductivity vs carrier concentration at T=300 K for different growth technologies, bibliographic data and results for samples under study: Fig. 2A MOVPE technique [18-23]; Fig. 2B MBE technique [5-10] and Fig. 2C HVPE technique [11-17].
Bibliographic data: red open circles correspond to Si-doping and blue full circles to Ge-doping; samples under study: red open stars correspond to Si-doping and blue full stars to Ge-doping. Figures with index 1 present the bibliographic data only and Figures with index 2 the comparison with results presented in this work (the bibliographic data points are smaller for clarity). Solid line corresponds to $\sigma(n)$ fitting proposed by Narita [4].

Otherwise, if the concentration is not negligible compared to the density of states of the conduction band, the carrier gas should be considered as degenerate and the Fermi-Dirac distribution f_o should be used instead for an accurate calculation. In a particular situation when the doping is so high that the Fermi level E_F is situated in the conduction band and $(\partial f_o)/\partial E \approx \delta(E-E_F)$ (where δ is the Dirac delta function) only the carriers with energy corresponding to the Fermi energy participated in the conduction process. Later in this paper this case will be referred to as "high degeneracy conditions". In Fig. 3 the position of the reduced Fermi energy: $(E_f-E_c)/kT$ vs free carrier concentration in GaN at room temperature is shown. The Fermi level merges the conduction band minimum for $n=2\times10^{18}cm^{-3}$ and the high degeneracy condition (usually considered for the case $(E_f-E_c)/kT\sim5$) should be expected for $n> 2\times10^{18}cm^{-3}$.

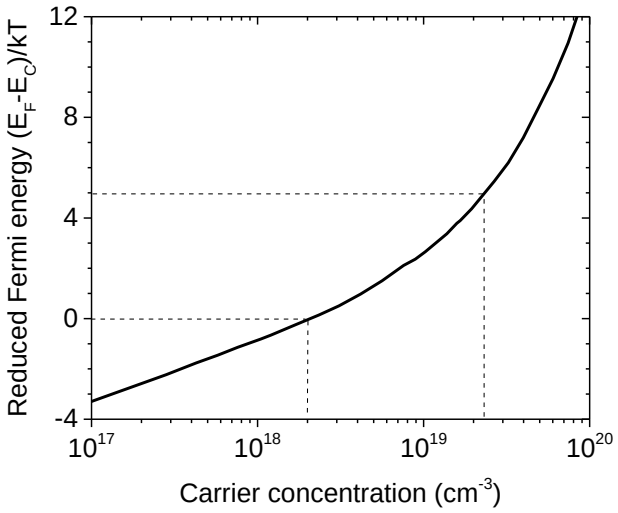

Fig. 3 The reduced Fermi energy: *(Ef-Ec)/kT* vs free carrier concentration in GaN at room temperature T=295K.

Usually, in the analysis of experimental results it is assumed for simplicity that the conditions of high degeneration are met and the r_H value is equal to 1. Details of this approximation are discussed in the Appendix.

The results of measurements of the Hall Effect indicated that for all the samples under study, the conduction process over the whole temperature range is identical and is related to the presence of free carriers in the conduction band. As an example, Fig. 4 presents the results of the Hall Effect as a function of the magnetic field for the sample H6 measured at three temperatures: 9 K, room temperature (295 K) and 645 K. For all three temperatures, the dependence of the Hall resistance on the magnetic field is perfectly linear with a practically identical slope.

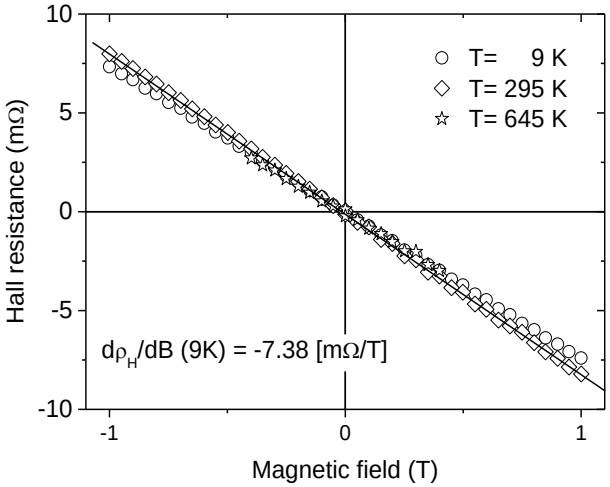

Fig. 4 Hall resistance V_H/I_s vs magnetic field at T=9 K, 295 K and 645 K respectively. Results for sample H6.

Typical results of the dependence of the Hall Effect on temperature are presented in Fig. 5 where the Hall concentration $n_{H=}e/R_H(T)$ is plotted vs temperature. As the character of the experimental $n_H(T)$ dependences for different types of samples are similar, the figure presents combined results for different growth technologies as well as for both types of dopants. In the whole studied range of carrier concentration, starting from the lowest, corresponding to the Mott transition in Si-doped crystals [1], no decrease in the carrier concentration, which could be related to the deionization of the donor impurity states, was observed. As expected, the free carrier concentration in the investigated samples can be considered as temperature independent. However, it should be noticed that for some samples the Hall concentration $n_H(T)$ shows a minimum around T=150 K. This effect is particularly well visible for sample P3 with the lowest carrier concentration. For other samples, the

minimum is either less visible or it does not exist at all. Assuming the real carrier concentration in the sample as independent of the temperature and taking into account formula (1) linking the Hall concentration n_H with the real concentration of carriers n, the observed effect can be explained by the dependence of the Hall scattering factor r_H on the temperature. If it is assumed that the results at low temperature T_{min} meet the criterion of high degeneracy (r_H=1), the variation of $r_H(T)$ can be determined as $r_H=n_H(T)/n_H(T_{min})$.

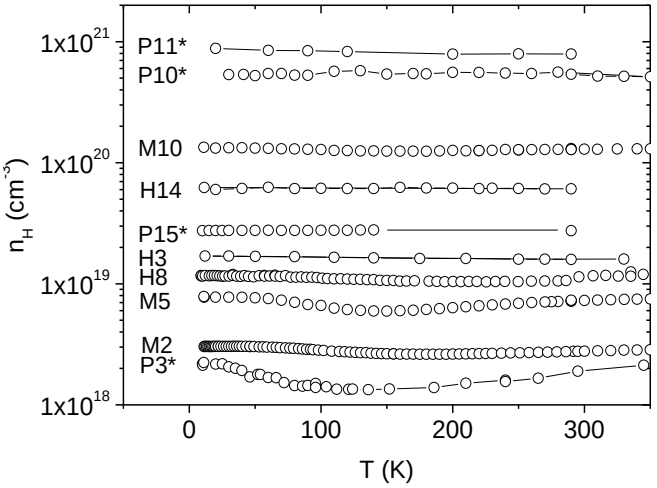

Fig. 5 Hall carrier concentration vs temperature for samples with different free carrier concentration (results for all three crystal growth technologies are presented).

Basing on such an approach, Fig. 6 shows r_H vs temperature dependence for a few selected samples. The character of the r_H(T) dependency is as expected (see Appendix). With decreasing the temperature, the value of the r_H factor increases due to the rising role of scattering on the ionized impurities. Then, as the conditions of the strong degeneracy are met, the r_H value sharply decreases and tends to a constant value. Of course, as it can be seen in Fig. 6, this effect is significant for low carrier concentrations and disappears as the concentration increases and meets the conditions of strong degeneracy even in the higher temperatures range. The results presented in Fig. 7 indicate that even for the carrier concentration as high as 10^{20} cm^{-3}, deviations from the strong degeneracy condition are of several percent. In the case of the temperature effect, for $n>10^{18}$ cm^{-3} one can consider the fulfillment of the strong degeneracy condition only at temperatures lower than 50 K.

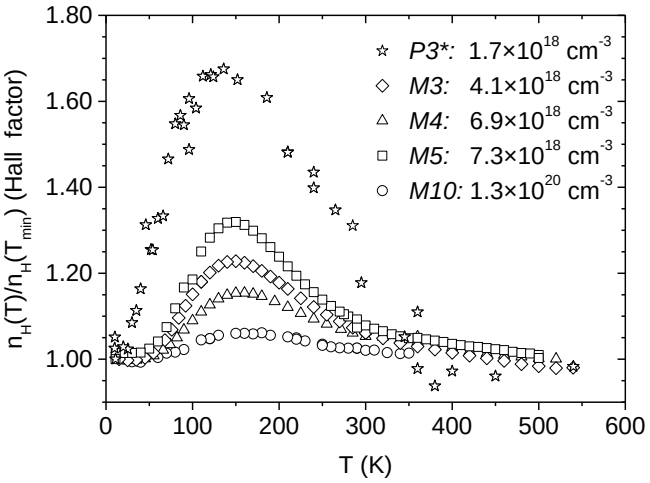

Fig. 6 $n_H(T)/n_H$(10 K) (Hall scattering factor) vs temperature. Results for samples:
P3* n=1.7×10^{18} cm^{-3}; M3 n=4.1×10^{18} cm^{-3};
M4 n=6.9×10^{18} cm^{-3}; M5 n=7.3×10^{18} cm^{-3} and
M10 n=1.3×10^{20} cm^{-3}.

Deviations from this behavior (for example sample M5 in Fig. 6) may be due to the fact that in different samples the effect of scattering by ionized impurities (the compensation level) as well as dislocations may vary in comparison to the same effect associated with phonon scattering. As an example in Fig. 7 two samples with the same carrier concentration but with different mobility are compared. For the sample characterized by a lower mobility value the r_H(T) variation is much weaker. Due to this lower mobility, it can be expected that one scattering mechanism, in this case on ionized impurities, dominates in the whole temperature range.

3.2.2 *Resistivity and mobility as a function of temperature*

Typical results of the dependence of resistivity on temperature are presented in Fig. 8 where the resistivity vs reciprocal of temperature is plotted. This figure presents the combined results for different growth technologies as well as for both types of dopants. Except for sample P3*, characterized by the lowest free carrier concentration, the resistivity is temperature

independent in the low temperature range. With increasing the temperature, the minimum of resistivity followed by its increase in the vicinity of room temperature is observed.

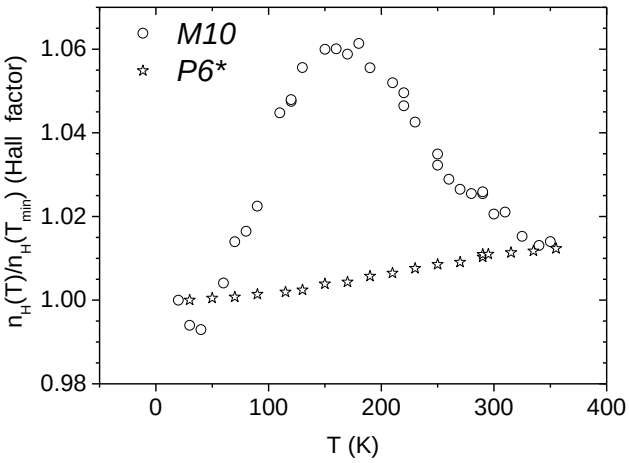

Fig. 7 n_H(T)/n_H(T_{min}) (Hall scattering factor) vs temperature. Results for samples M10 and P6* characterised at 300 K by:
circles: M10 n=1.3×10^{20} cm^{-3} and μ=120 cm²/Vs
stars: P6* n=1.2×10^{20} cm^{-3} and μ=88 cm²/Vs

This effect becomes more pronounced as the sample low temperature resistance increases. The relationship between the sample resistivity ρ and the carrier mobility μ in the material is given by a simple formula:

$$\rho = \frac{1}{en\mu} \qquad (3)$$

Taking into account the discussion in the previous chapter, the carrier concentration n in the investigated samples can be assumed as temperature independent and equal to the Hall concentration value at low temperature. Consequently, the carrier mobility value can be determined directly from the reciprocal of the resistivity value according to the formula:

$$\mu(T) = \frac{1}{en(T_{min})} \cdot \frac{1}{\rho(T)} \qquad (4)$$

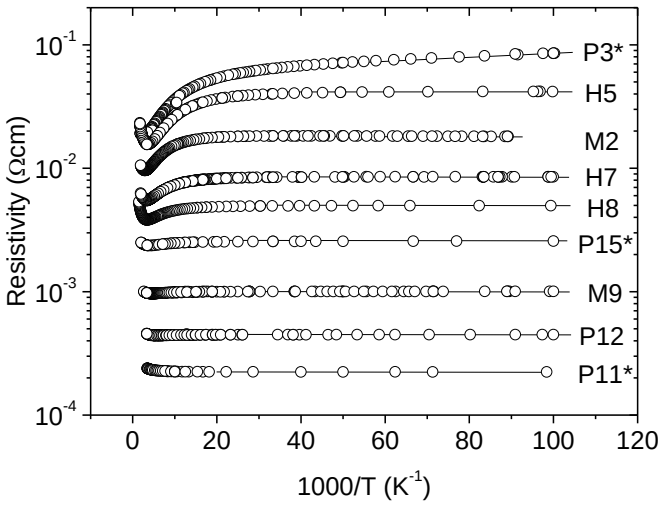

Fig. 8 Resistivity vs reciprocal of temperature variation for samples with different free carrier concentration (results for all three crystal growth technologies are presented).

Mobility values of the investigated samples, determined from formula (4), are shown in Fig. 9A (results at room temperature) and Fig. 9B (the low-temperature case for T=11 K).

With the exception of the samples with very high carrier concentration (n>2×10^{20} cm^{-3}), the mobility values determined at room temperature correspond to the $\mu(n)$ dependence expected on the basis of the analytical equations from paper [31]. Meanwhile, the values of mobility measured at low temperatures, equal to about 100 cm²/Vs, practically do not depend either on the carrier concentration or on the growth technology.

The character of μ(T) dependencies in the whole investigated temperature range is shown in Fig. 10. In principle, three types of behavior can be distinguished. Samples presented in Fig. 10A are characterized by the carrier concentration n>6×10^{19} cm^{-3}. For these samples, in practically the whole investigated temperature range, the mobility is constant and independent on the temperature. Only in the vicinity and above room temperature a slight decrease of the mobility value is observed. Figure 10B shows the results for samples with a carrier concentration n<1×10^{19} cm^{-3}. For these samples, in the temperature range up to approximatively 70 K, the mobility is constant, independent on the

temperature. Then it increases with increasing the temperature, passes through a maximum near room temperature and drops sharply in the higher temperature range. Figure 10C presents the $\mu(T)$ dependence for sample P3*. A maximum of $\mu(T)$ is also observed, but otherwise the mobility monotonically changes as a function of temperature without any plateau range.

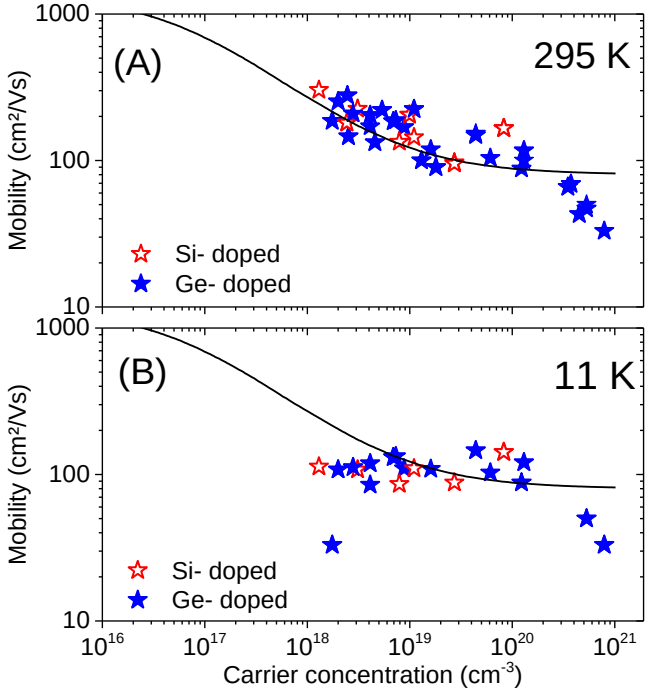

Fig. 9 Mobility as a function of carrier concentration. Si-doped samples: open, red stars and Ge-doped ones: full, blue stars. Solid line corresponds to $\mu(n)$ mobility model for bulk GaN at 295 K [31].
(9A): results at 295 K for all samples in accordance with Tab. I; (9B): results at 11 K for samples measured as a function of temperature ("yes" in column "Study of T-dependency" of Tab. I).

While the qualitative description of the maximum of $\mu(T)$ dependency in the vicinity of room temperature is easy to understand as it is related to the competition between two dominant scattering mechanisms described as: $\mu_{cc} \propto T^{+3/2}$ for ionized impurities and $\mu_{ph} \propto T^{-3/2}$ for phonons, the temperature independence in the low temperature range where μ_{cc} dominates is not obvious.

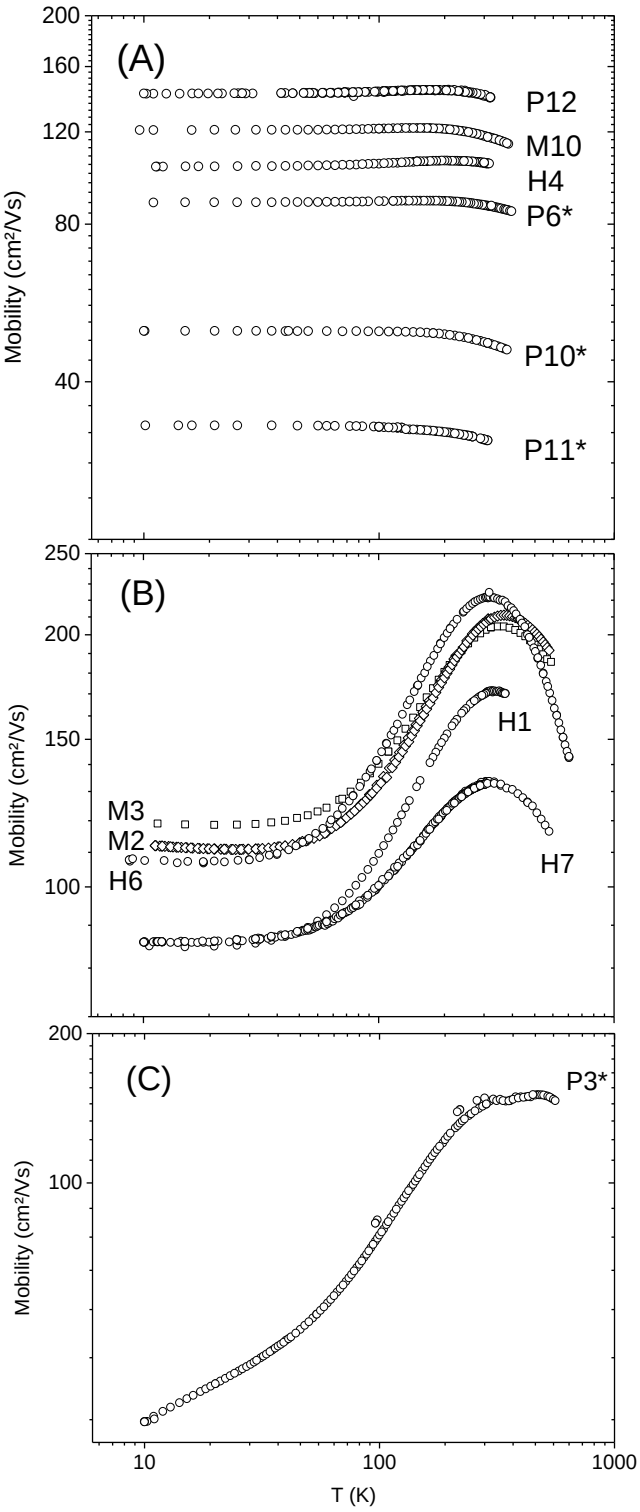

Fig. 10 Mobility as a function of temperature measured for:
(Fig.10A): samples with carrier concentration n>6x10^{19} cm^{-3}; (Fig.10B): samples with carrier concentration $2\times10^{18}<n<8\times10^{18}$ cm^{-3}; (Fig. 10C): sample P3* with n=1.7×10^{18} cm^{-3}.

The standard textbook approach [24] for dealing with ionized impurity scattering in semiconductors is the Brook–Herring (BH) model. It is based on two inherent approximations: Born approximation and single ion screening approximation. This can lead to a poor fit to the experimental mobility, especially at higher electron concentrations. An analytic treatment based on the phase-shift analysis (P-SA) [32] takes into account the multi-ion screening effect and overcomes both the approximations. The temperature dependence of the electron mobility in GaN, calculated within the both mentioned models, has been presented in paper [24]. Figure 11 shows the results of these calculations made for ionized donor concentrations of 1×10^{18} and 1×10^{19} cm^{-3} with a 20% compensation. As it can be seen, both theoretical BH and P-SA models predict a strong dependence of mobility on temperature in the whole studied low temperature range. Such variation is not observed experimentally in the investigated samples, for which the mobility does not depend on the temperature at all, or only in the low-temperature range. For comparison the experimental results for less doped H5 and P3* samples are presented in Fig. 11. In the standard textbook approach of BH model, the Fermi–Dirac distribution function is considered, so both non-degenerate and degenerate cases are included. However in paper [33] the simple formula of BH model in the particular case of high degeneracy has been proposed:

$$\mu_{cc} = \frac{24\pi^3\varepsilon^2\hbar^3 n}{e^3 m^{*2} N_{ion}\left[ln[1+\gamma(n)]-\frac{\gamma(n)}{1+\gamma(n)}\right]} \qquad (5)$$

where $\gamma(n) = \frac{4\sqrt[3]{3}\pi^{8/3}\hbar^2\varepsilon n^{1/3}}{e^2 m^*}$

In Eq. 5 ε is the static dielectric constant (ε= 9.5ε$_0$ [24]), m* - the effective mass (m^*= 0.22m$_0$ [33]), N_{ion} - concentration of ionised scattering centres and π and $\hbar$ have their usual meanings.

As it can be seen from Eq. 5, in contrast to the nondegenerate case, there is no explicit temperature dependence and the concentration of scattering centres N_{ion} appears only through the compensation N_{ion}/n. Consequently, as can be seen in Fig. 11, in the case of high degeneracy, the scattering on ionized impurities becomes temperature independent and much less dependent on the dopant concentration (in the case of constant compensation this dependency appears only through the functions γ(n)).

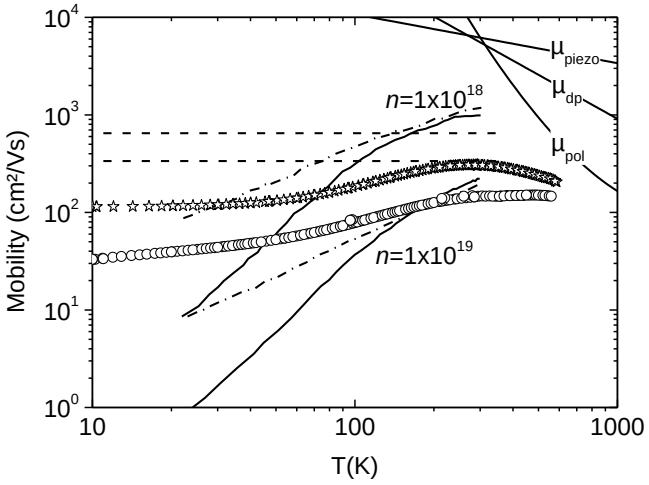

Fig. 11 Mobility as a function of temperature. Experimental points:
stars - sample H5 (n=1.3×10^{18} cm^{-3});
circles - sample P3* (n=1.75×10^{18} cm^{-3}).

Theoretical curves for ionized donor concentrations of 10^{18} cm^{-3} (upper curve) and 10^{19} cm^{-3} (lower curve) with 20% compensation [24]: solid lines BH model; dashed-dot lines P-SA one; dashed lines high degeneracy case of BH model [33].

For illustration, also the mobility values for: phonon acoustic scattering [24] (μ$_{piezo}$-piezoelectric mode and μ$_{dp}$- deformation potential mode) as well as μ$_{pol}$-polar phonon scattering [34] are shown.

It should be noted that both samples shown in Fig. 11 and characterized by a stronger μ(T) dependency have the lowest carrier concentration near the boundary of the Mott transition. In this case the conduction effects related to the presence of donor states should be considered. The hopping conduction mechanism can be discarded because it can be expected for carrier concentrations n<1×10^{18} cm^{-3} but most of all because it is accompanied by the vanishing of Hall effect [35]. Whereas, as it was signaled in Chapter 3.2.1 and shown in Figure 4, for all the samples under study the Hall effect in the

whole temperature range was measurable and perfectly linear as a function of the magnetic field. Another possibility that should be considered is the process of diffusive conduction in shallow impurities due to the small but finite overlap of the localized electron wave function of the defect centers [36]. Such an effect would manifest itself and be described as conductivity in a parallel layer. Also in this case, measurements of the Hall effect being perfectly linear as a function of magnetic field, indicate that the conduction process takes place in the conduction band and that only one type of carriers participates in electrical conductivity. Unfortunately, if the parameters of the conduction process in the impurity band are similar to those of the conduction band, then the slight changes in the resistance and Hall effect in the investigated samples do not allow to estimate whether this effect actually takes place. Perhaps examining more samples with concentrations of the range of 1-3×10^{18} cm^{-3} would provide more information to investigate this phenomenon. However, it is worth noting that an analysis of a similar effect in GaAs [37] leads to the conclusion that the mobility value determined in the experiment can be identified with the carrier mobility in the conduction band only at room temperature. At lower temperatures the experimental mobility values are systematically too low when compared with the true mobility in the conduction band. This means that for samples H5 and P3 * the real dependence of the mobility in the conduction band on temperature would be even weaker compared to the μ (T) curve in Fig. 11.

Analyzing the possible mechanisms of carrier scattering, in principle, one can also consider the possibility of scattering on dislocations. The mobility related to edge dislocation scattering in a parabolic approximation and under high degeneracy conditions can be written in the following form [33]:

$$\mu_{disloc} = \frac{4 \cdot 3^{2/3} e c^2 n^{2/3}}{\pi^{8/3} \hbar N_{dis}} [1 + \gamma(n)]^{3/2} \qquad (6)$$

In Eq. 6 N_{dis} is the concentration of dislocations and c=5,185 (Å) [38] is the lattice constant. A comparison of both mechanisms can be seen in Fig. 12. The dislocation scattering is strongly dependent on the carrier concentration and, therefore, even at high dislocation concentration N_{dis} scattering quickly becomes negligibly weak. As it is seen from Eq. 6, the scattering by dislocations is, similar to the case of ionized impurities, temperature independent.

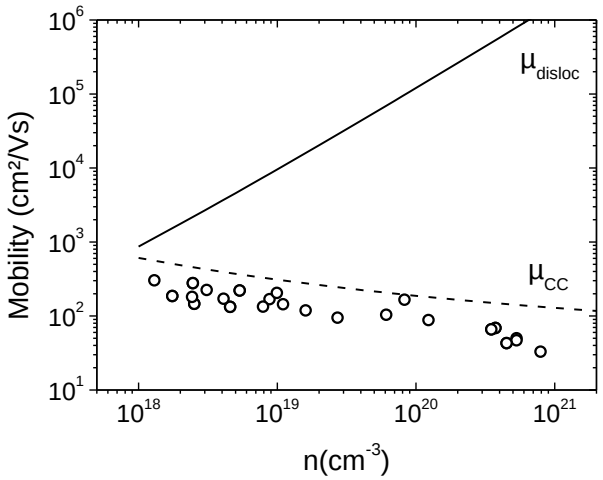

Fig. 12 Mobility as a function of carrier concentration according to the model from paper [33]: solid line – theory for dislocation scattering with N_{dis}=1×10^{10} cm^{-2}; dashed line - ionized impurities scattering with 20% compensation. Circles - experimental mobility for samples under study at T=295 K.

4. Summary

In this paper, the results of low temperature resistivity and Hall Effect measurements of Ge and Si-doped GaN grown by PAMBE, HVPE, and MOVPE have been presented. Although the literature data indicate that the Ge-doped samples are generally characterized by lower mobility and/or lower conductivity than those doped with Si, in the set of samples in this paper, the applied technological processes allowed to obtain materials with very similar parameters, regardless of the type of donor atoms introduced. A clear difference appears in the case of doping level above n=1×10^{20} cm^{-3}, where obtaining such high concentrations is possible only in the case of doping with Ge.

The behavior of the Hall scattering factor r_H as a function of temperature allows to assess that the electron carrier gas in GaN at room temperature can be considered as fully degenerate only for concentrations higher than $n>1\times10^{20}$ cm^{-3}. Below this concentration, the r_H parameter is temperature dependent, indicating that the condition $r_H=1$, the correct one for the case of strong degeneracy, is not fulfilled. As the temperature is lowered, for most samples r_H becomes temperature independent only at temperatures below the temperature of liquid nitrogen. An exception is sample P3* with the lowest carrier concentration $n=1.75\times10^{18}$ cm^{-3} for which this condition is met only at the temperature as low as 25 K.

The high degeneracy criterion is crucial for the analysis of the mobility behavior of μ *(T)* at temperatures below room temperature, where the ionized scattering mechanism becomes the dominant one. The standard textbook BH expression, though very widely used, breaks down for the highly doped material under study. The improved method that takes advantage of the phase shift analysis of electron–impurity scattering and deals with multi-ion screening does not explain the experimentally observed independence of mobility on temperature for temperatures below 70 K. The explanation of the observed $\mu(T)$ variation in the whole investigated temperature range could be related to the transition, as a function of temperature, to the strong degeneracy condition and the necessity to use the formulas applicable for this particular case.

Acknowledgments

The authors acknowledge the support from the GANEX (No. ANR-11-LABX-0014 GANEX belongs to the publicly funded "Investissements d'Avenir" program managed by the French ANR agency) as well as from the Polish National Science Center through Project No. 2020/37/B/ST5/03746.

Appendix

The conductivity tensor can be noted as follows:

$$\hat{\sigma} = \begin{bmatrix} \sigma_{xx} & \sigma_{xy} & 0 \\ -\sigma_{xy} & \sigma_{xx} & 0 \\ 0 & 0 & \sigma_{zz} \end{bmatrix} \quad \text{(A1)}$$

When mutually perpendicular electrical and magnetic field (Hall Effect configuration) are impressed on a conductor, in the case of one type of carriers the components of the tensor are respectively:

$$\sigma_{xx} = \frac{e^2 n}{m^*}\left\langle\frac{\tau}{1+s^2}\right\rangle \quad \text{(A2)}$$

$$\sigma_{xy} = \frac{e^2 n}{m^*}\left\langle\frac{s\tau}{1+s^2}\right\rangle \quad \text{(A3)}$$

$$\sigma_{zz} = \frac{e^2 n}{m^*}\langle\tau\rangle \quad \text{(A4)}$$

and the parameter *s* corresponds to:

$$s = \frac{e\tau}{m^*}B = \mu B \quad \text{(A5)}$$

with carrier charge *e*, its effective mass *m**, mobility μ, relaxation time for scattering process τ. B correspond to the magnetic field.

As a consequence the Hall resistivity (in the direction perpendicular to the current) is given as:

$$\rho_H = R_H B = -\rho_{xy} = \frac{\sigma_{xy}}{\sigma_{xx}^2+\sigma_{xy}^2} \quad \text{(A6)}$$

As a function of the applied magnetic field intensity two cases can be considered:

(i) High magnetic field or $s=\mu B>>1$:

In this case formula (A6) can be simplified into:

$$R_H \cong \frac{1}{B}\cdot\frac{1}{\sigma_{xy}} \cong \frac{1}{B}\cdot\frac{B}{en} = \frac{1}{en} \quad \text{(A7)}$$

Consequently, in the case of sufficiently high magnetic field the free carrier concentration can be determined directly from the Hall Effect measurement. Unfortunately, this condition can be met only for materials with very high mobility ($\mu>>10000 cm^2/Vs$). For typical mobility in GaN and magnetic field of the order of 1 T, the value of the parameter s does not exceed 0.1, so it corresponds to the second case:

(ii) Low magnetic field or $s=\mu B<<1$:

In this case formula (A6) can be simplified into:

$$R_H \cong\cong \frac{1}{B}\cdot\frac{\sigma_{xy}}{\sigma_{xx}^2} \cong \frac{1}{en}\frac{\langle\tau^2\rangle}{\langle\tau\rangle^2} = \frac{r_H}{en} \qquad \text{(A8)}$$

Therefore, in the case of a weak magnetic field, the concentration of free carriers can be determined from the Hall Effect only with the accuracy to the proportionality factor r_H, called the "Hall scattering factor":

$$r_H = \frac{\langle\tau^2\rangle}{\langle\tau\rangle^2} \qquad \text{(A9)}$$

The average value ⟨X⟩ in formula (A9) depends on the details of the band structure and all the carrier scattering mechanisms in the material. However, the situation is particularly simple when high degeneracy can be assumed. In this case the average value of a function corresponds to its value on the Fermi level and consequently the Hall factor r_H is equal to 1. In all other cases, the Hall factor value should be calculated or at least estimated.

TABLE AI: Hall factor, r_H value for different scattering modes:

Scattering process mode	r_H value
Acoustic phonons by deformation potential	1.18
Acoustic phonons by piezoelectric mode	1.10
Alloy	1.18
Neutral impurity	1
Ionized impurity	1.93
Nonpolar optical phonons	1.18
Polar optical phonons	1.10

If one considers a nondegenerate semiconductor with a parabolic band with a spherical constant energy surface and assumes that the scattering mechanisms are elastics and can be described by the relaxation time expressed in the form of $\tau\sim E^{\alpha}$ (where α is the scattering event dependent parameter), then the Hall factor can be easily calculated as combinations with Gamma Euler functions of parameter α. The results are presented in Tab. AI [24]. Optical phonon scattering, as inelastic and anisotropic is the one for which the relaxation time cannot be defined. However, the advantages of describing the complex scattering process by relaxation time are overwhelming enough to develop, not completely accurate by closed form, analytical solutions for relaxation time approximation in this case as well. The scattering parameter α determined this way allowed to complete Tab. AI with the case of scattering on polar and non-polar optical phonons. As can be seen from Tab. AI, in the case of a weak degeneracy and the dominant scattering mode on ionized impurities, the experimentally determined carrier concentration may be nearly twice lower than the real concentration of carriers in the material. In the case of other scattering mechanisms, this effect is correspondingly weaker. It should also be noted that due to the different dependence of the dispersion mechanisms on temperature, their participation in the total relaxation time changes with temperature, which leads to the dependence of the Hall factor on temperature and could mask real changes in the actual carrier concentration. As an example, Fig. 13 shows the temperature variation of the Hall factor for n-type GaN with the carrier concentration $n=1\times10^{17}$ cm^{-3}.

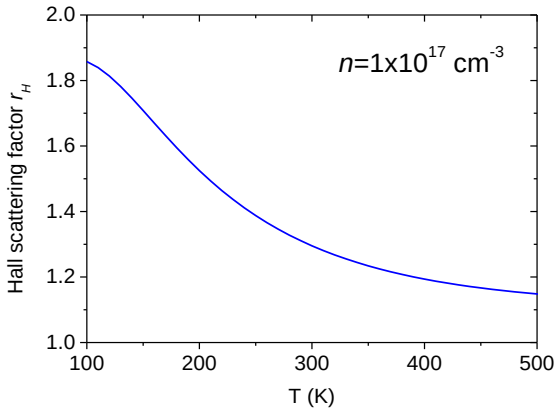

Fig. 13 Hall scattering factor r_H vs temperature. Modelling for *n*-GaN with free carrier concentration 1×10^{17} cm^{-3}

References

[1] A. Wolos, Z. Wilamowski, M. Piersa, W. Strupinski, B. Lucznik, I. Grzegory, and S. Porowski 2011 *Phys. Rev.* B **83** 165206
[2] M.B. C. Nenstiel G. Callsen, F. Nippert, T. Kure, S. Fritze, A. Dadgar, H. Witte, J. Bläsing, A. Krost, and A. Hoffmann 2015 *Phys. Status Solidi RRL* **9** 716
[3] J.N. Baker and J.S.H. P.C. Bowes R. Collazo, Z. Sitar, and D.L. Irving 2020 *Applied Physics Letters* ***117*** 102109
[4] T. Narita, T. Kachi, *Characterization of Defects and Deep Levels for GaN Power Devices:* 2020 *AIP Publishing*
[5] A. Ajay, J. Schörmann, M. Jiménez-Rodriguez, C.B. Lim, F. Walther, M. Rohnke, I. Mouton, L. Amichi, C. Bougerol, M.I. Den Hertog, M. Eickhoff, and E. Monroy 2016 *J. Phys. D: Appl. Phys.* **49** 445301
[6] E.C.H. Kyle, S.W. Kaun, P.G. Burke, F. Wu, Y.-R. Wu, and J.S. Speck 2014 *Journal of Applied Physics* **115** 193702
[7] F. Afroz Faria, J. Guo, P. Zhao, G. Li, P. Kumar Kandaswamy, M. Wistey, H. (Grace) Xing, and D. Jena 2012 *Appl. Phys. Lett.* **101** 032109
[8] L. Lugani, M. Malinverni, S. Tirelli, D. Marti, E. Giraud, J.-F. Carlin, C.R. Bolognesi, and N. Grandjean 2014 *Appl. Phys. Lett.* **105** 202113
[9] M.N. Fireman, G. L'Heureux, F. Wu, T. Mates, E.C. Young, and J.S. Speck 2019 *Journal of Crystal Growth* **508** 19.
[10] P.R. Hageman, W.J. Schaff, J. Janinski, and Z. Liliental-Weber 2004 *Journal of Crystal Growth* **267** 123
[11] P.P. Paskov, M. Slomski, J.H. Leach, J.F. Muth, and T. Paskova 2017 *AIP Advances* **7** 095302
[12] Y.-M. Zhang, J.-F. Wang, D.-M. Cai, G.-Q. Ren, Y. Xu, M.-Y. Wang, X.-J. Hu, and K. Xu 2020 *Chinese Phys.* B **29** 026104
[13] B. Wang, P. Yu, B. Kucukgok, A.G. Melton, N. Lu, and I.T. Ferguson 2014 *Phys. Status Solidi C* **11** 573
[14] Y. Oshima, T. Yoshida, K. Watanabe, and T. Mishima 2010 J*ournal of Crystal Growth* **312** 3569
[15] Y. Oshima, T. Yoshida, T. Eri, M. Shibata, and T. Mishima 2007 *Phys. Stat. Sol. C* **4** 2215
[16] E. Richter, Ch. Hennig, U. Zeimer, L. Wang, M. Weyers, and G. Tränkle 2006 *Phys. Stat. Sol. A* **203** 1658
[17] S. Xia, Y. Zhang, J. Wang, J. Chen, and K. Xu 2021 S*emicond. Sci. Technol.* **36** 014009
[18] S. Fritze, A. Dadgar, H. Witte, M. Bügler, A. Rohrbeck, J. Bläsing, A. Hoffmann, and A. Krost 2012 *Appl. Phys. Lett.* **100** 122104
[19] D. Schiavon, E. Litwin-Staszewska, R. Jakieła, S. Grzanka, and P. Perlin 2021 *Materials* **14** 354
[20] I. Halidou, Z. Benzarti, Z. Chine, T. Boufaden, and B. El Jani 2001 *Microelectronics Journal* **32** 137
[21] X. Liu, L. Wang, D.-C. Lu, D. Wang, X. Wang, and L. Lin 1998 *Journal of Crystal Growth* **189–190** 287
[22] N.G. Young, R.M. Farrell, M. Iza, S. Nakamura, S.P. DenBaars, C. Weisbuch, and J.S. Speck 2016 *Journal of Crystal Growth* **455** 105
[23] R. Kirste, M.P. Hoffmann, E. Sachet, M. Bobea, Z. Bryan, I. Bryan, C. Nenstiel, A. Hoffmann, J.-P. Maria, R. Collazo, and Z. Sitar 2013 *Appl. Phys. Lett.* **103** 242107
[24] Morkoç Hadis, *Handbook of Nitride Semiconductors and Devices* 2008 *WILEY-VCH Verlag GmbH & Co. KGaA, Weinheim*
[25] H. Turski, G. Muzioł, M. Siekacz, P. Wolny, K. Szkudlarek, A. Feduniewicz-Żmuda, K. Dybko, and C. Skierbiszewski 2018 *Journal of Crystal Growth* **482** 56
[26] W.K. Fong, C.F. Zhu, B.H. Leung, C. Surya, B. Sundaravel, E.Z. Luo, J.B. Xu, and I.H. Wilson 2002 *Microelectronics Reliability* **42** 1179
[27] R. Dwiliński, R. Doradziński, J. Garczyński, L.P. Sierzputowski, A. Puchalski, Y. Kanbara, K. Yagi, H. Minakuchi, and H. Hayashi 2008 *Journal of Crystal Growth* **310** 3911
[28] M. Iwinska, T. Sochacki, M. Amilusik, P. Kempisty, B. Lucznik, M. Fijalkowski, E. Litwin-Staszewska, J. Smalc-Koziorowska, A. Khapuridze, G. Staszczak, I. Grzegory, and M. Bockowski 2016 *Journal of Crystal Growth* **456** 91
[29] M. Iwinska, N. Takekawa, V.Yu. Ivanov, M. Amilusik, P. Kruszewski, R. Piotrzkowski, E. Litwin-Staszewska, B. Lucznik, M. Fijalkowski, T. Sochacki,

H. Teisseyre, H. Murakami, and M. Bockowski 2017 *Journal of Crystal Growth* **480** 102
[30] M. Levy and M.P. Sarachik 1989 *Review of Scientific Instruments* **60** 1342
[31] F. Schwierz 2005 *Solid-State Electronics* **49** 889
[32] J.R. Meyer and F.J. Bartoli 1987 *Phys. Rev. B* **36** 5989
[33] D.C. Look, C.E. Stutz, R.J. Molnar, K. Saarinen, and Z. Liliental-Weber 2001 *Solid State Communications* **117** 571
[34] B.K. Ridley, Quantum Processes in Semiconductors p.128 (Clarendon Press, Oxford, 1999)
[35] D.C.Look D. C. Reynolds, W. Kim, Ö. Aktas, A. Botchkarev, A. Salvador, and H. Morkoç 1996 *Journal of Applied Physics* **80**, 5, 2960
[36] R.J.Molnar T. Lei, and T. D. Moustakas 1993 *Applied Physics Letters* **62**, 72
[37] H.Neuman, 1988 *Crystal Research and Technology*, **23**, 1377
[38] Leszczynski, M.; Suski, T.; Teisseyre, H.; Perlin, P.; Grzegory, I.; Jun, J.; Porowski, S.; Moustakas, T. D. 1994 *Journal of Applied Physics*, **76,** 8, 4909